

RSC Advances

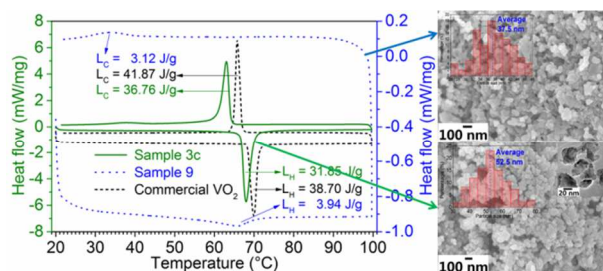


This is an *Accepted Manuscript*, which has been through the Royal Society of Chemistry peer review process and has been accepted for publication.

Accepted Manuscripts are published online shortly after acceptance, before technical editing, formatting and proof reading. Using this free service, authors can make their results available to the community, in citable form, before we publish the edited article. This *Accepted Manuscript* will be replaced by the edited, formatted and paginated article as soon as this is available.

You can find more information about *Accepted Manuscripts* in the [Information for Authors](#).

Please note that technical editing may introduce minor changes to the text and/or graphics, which may alter content. The journal's standard [Terms & Conditions](#) and the [Ethical guidelines](#) still apply. In no event shall the Royal Society of Chemistry be held responsible for any errors or omissions in this *Accepted Manuscript* or any consequences arising from the use of any information it contains.



Freeze drying was employed to produce highly pure and crystalline thermochromic VO₂ nanoparticles. By changing the precursor concentration and annealing temperature, particle size and crystallinity can be controlled. With 7.5 mL H₂O₂ in the solvent, the sample annealed at 650 °C simultaneously achieved high crystallinity comparable to the purchased commercial powder (36.76 vs 41.87 J/g latent heat) and a small average size of 52.5 nm.

ARTICLE

Solution-Based Fabrication of VO₂ (M) Nanoparticles via Lyophilisation

Cite this: DOI: 10.1039/x0xx00000x

Xun Cao,^a Myat Noe Thet,^a Yu Zhang,^b Say Chye Joachim Loo,^{ac} Shlomo Magdassi,^d Qingyu Yan^{abe} and Yi Long^{*a}

Received 00th January 2015,
Accepted 00th February 2015

DOI: 10.1039/x0xx00000x

www.rsc.org/

Thermochromic vanadium dioxide (VO₂) is the most extensively researched smart material owing to its near room-temperature phase transition at around 68 °C. Freeze drying has been employed in the solution-based fabrication of highly pure and crystalline VO₂ nanoparticles and it was found that freeze drying can largely eliminate the agglomeration issue which is common in nanoparticle fabrication. The particle size, phase transition temperature (τ_c), crystallinity and latent heat (L_H) have been systematically studied by changing the precursor concentration and annealing temperature. The freeze-dried sample (with 7.5 mL H₂O₂ in precursor) annealed at 650 °C has a particle size of ~ 53 nm and τ_c of 64.5 °C, as well as high crystallinity with LC of 36.76 J/g.

Introduction

Vanadium dioxide (VO₂) undergoes fully reversible metal-insulator transitions (MIT) from semiconducting monoclinic phase to metallic rutile phase at the critical temperature (τ_c) of 68 °C.^{1, 2} The MIT is observed by a sharp change in infrared (IR) transmittance and electrical resistivity within 500 fs.³ While τ_c is adjustable to room temperature via doping,^{4, 5} VO₂ has thus become a suitable candidate in a wide range of potential applications, including energy-saving thermochromic smart windows,⁶ IR uncooled bolometers,⁷ sensors,^{8, 9} field effect transistors¹⁰ and optical storage devices.¹¹⁻¹³

Thermochromic VO₂ faces the drawback of low luminous transmittance (T_{lum}) and low solar modulating ability (the ability to regulate the input solar energy, ΔT_{sol}). Enhancing both properties poses a great challenge and recent researches have focused on embedding VO₂ NPs (NPs)/matrix composite foils,^{14, 15} and thin film nanostructuring such as bio-inspired VO₂ with anti-reflection (AR) effects¹⁶ and controlled nanoporosity.¹⁷ Although the newly developed organic¹⁸ and hybrid¹⁹ smart system based on temperature-responsive hydrogel matrix gave unprecedented thermochromic performance, the translucent appearance at higher temperature limited its full application in the field of smart windows.

Synthesis of VO₂ NPs has been extensively studied and the resultant particle sizes, morphologies and phase transition temperatures are listed in **Table 1**. Two major fabrication methods include mechanical milling¹⁴ and hydrothermal synthesis,^{15, 20} which could produce NPs with size less than 100 nm. One of the intrinsic issues of mechanical milling hindering its full application is the large size variation and distribution of the produced NPs, while hydrothermal methods mainly suffers from safety issues related with potential explosion of expensive autoclaves and difficulties in scaling up.

Freeze drying has been a well-established process in chemical synthesis and food processing industries, during which solvents are frozen at low temperature and sublime under low pressure, hence being removed in a vacuum environment. The synthesis of nanoporous SiO₂ and Al₂O₃ cryogels have also been reported in recent literatures,²⁷⁻³³ in which lyophilisation was employed to leave the nanoparticle suspensions intact.³⁴ During freeze drying, as there is no liquid-to-gas phase transformation, particles are not subjected to capillary force, and thus agglomeration of the NPs is reduced. In this study, we report a simple and reproducible solution-based fabrication method via freeze drying, which produced fine crystalline VO₂ (M) NPs and reduced phase transition temperature.

Table 1 A summary of ways to fabricate VO₂ NPs and their properties

Reported approaches	Particle size / shape	τ_c
Bead milling of commercial VO ₂ powder ¹⁴	~ 20 nm / irregular shape with core-shell structure	N. A.
Hydrothermal (V ₂ O ₅ -N ₂ H ₄ ·HCl) ¹⁵	25-45 nm / irregular shape	63.3 °C
Hydrothermal (V ₂ O ₅ -H ₂ C ₂ O ₄) ²⁰	~ 50 nm / spherical	55.7-55.9 °C
Pyrolysis of [NH ₄] ₅ [(VO) ₆ (CO ₃) ₄ (OH) ₉]·10H ₂ O precursor ²¹	N.A. / spherical	68.0-70.9 °C
Hydrothermal (V ₂ O ₅ -H ₂ C ₂ O ₄) with W-doping ²²	30-50 nm / N. A.	N. A.
Hydrothermal (V ₂ O ₅ -H ₂ C ₂ O ₄) with F-doping ²³	~ 30 nm / N. A.	35 °C (2.93% F)
Hydrothermal (V ₂ O ₅ -H ₂ C ₂ O ₄ -additives) ²⁴	~ 70 nm / spherical	32.2-69.6 °C
Hydrothermal (V ₂ O ₅ -N ₂ H ₄) ²⁵	< 20 nm / spherical	55.5 °C
Thermolysis of vanadyl ethylene glycolate (VEG) precursor ²⁶	50-100 nm / spherical	68.0 °C

ARTICLE

Experimental section

The chemicals used in this study were vanadium (V) oxide (V_2O_5 , 99.99%, Alfa Aesar), hydrogen peroxide (H_2O_2 , 30 wt%, VWR) and hydrazine monohydrate ($N_2H_4 \cdot H_2O$, 98%, Sigma-Aldrich), polyvinylpyrrolidone (PVP, 99%, Sigma-Aldrich) and ethanol (95%, Aik Moh). All of the chemicals were used as received without any further purification.

Synthesis of VO_2 (M) NPs and casting of VO_2 foil

182 mg of V_2O_5 powder was dissolved in different volumes of H_2O_2 and vigorously stirred at 70 °C for 2 h to form a reddish-brown sol. Following that, an appropriate amount of hydrazine was added and particles started to precipitate. The mixture was further stirred at 70 °C for another hour to facilitate full redox reaction. The as-prepared precursor was transferred into a 15 mL centrifuge tube (Corning Inc.), which was covered with a piece of filter paper and tightly sealed using parafilm. It was then placed in a 300 mL freeze drying flask (Fisher Scientific) and frozen in liquid nitrogen for 5 min. After that, it was quickly loaded onto the FreeZone 2.5 Plus lyophiliser (Labconco, USA) for 72 h of freeze drying to completely drive off the solvent. The lyophiliser collector was set at -80 °C and 0.01 mbar.

After freeze drying, the raw precursor powder was immediately removed from the centrifuge tube and transferred into a high purity quartz bottle (99.99% SiO_2 , Youlab), evenly distributed and annealed at 550 °C for 2 h in a tube furnace with argon (99.9995%, NOX) atmosphere. The ramping rate was set to 1.0 °C/min, and gas flow rate was tuned to around 200 cm^3/min .

A comparative sample was made via conventional drying method (centrifugation at 10000 rpm for 10 min), followed by drying in vacuum at room temperature before heat treatment.

The as-synthesised NPs and PVP (acting as dispersant to distribute NPs) were added to ethanol with the aid of Vortex-Genie 2 mixer (Scientific Industries, USA) and ultrasonication. The homogeneous dispersion was casted onto a piece of pre-cleaned microscopic glass slide.

Characterization method

The phases of the samples were determined with an XRD-6000 X-ray diffractometer (XRD, Shimadzu, Japan), of which the $Cu-K\alpha$ radiation was produced at 40 kV and 30 mA with $\lambda \approx 0.15406$ nm at an X-ray grazing angle of 1.0°. The phase transition of VO_2 (M) NPs was studied using a nitrogen-protected Q10 differential scanning calorimeter (DSC, TA Instruments, USA). The microstructures and the energy-dispersive X-ray spectroscopy (EDX) elemental mapping of the samples were characterised using a JSM-7600F field emission scanning electron microscope (FESEM, JEOL, Japan) with an INCA® EDX attachment (Oxford Instruments, UK), which was operated at an accelerating voltage of 5 kV under secondary electron imaging (SEI) mode and 20 kV for EDX respectively. The

morphology, selected area electron diffraction (SAED) pattern and high resolution transmission electron microscopy (HRTEM) images were obtained by a JEM-2010F field-emission gun transmission electron microscope (FEG-TEM, JEOL, Japan) operated at an accelerating voltage of 200 kV. The transmittance spectra and hysteresis loop were collected using a Cary 5000 ultraviolet-visible light-near infrared (UV-Vis-NIR) spectrophotometer (Agilent, USA), which was equipped with a PE120 peltier system simple heating and cooling stage (Linkam, UK). The calculations of integrated T_{lum} ($380 \leq \lambda \leq 780$ nm) and ΔT_{sol} ($280 \leq \lambda \leq 2500$ nm) can be found in equations (1) and (2) respectively.

$$T_{lum/sol}(\tau) = \frac{\int \phi_{lum/sol}(\lambda) \cdot T(\lambda, \tau) d\lambda}{\int \phi_{lum/sol}(\lambda) d\lambda} \quad (1)$$

$$\Delta T_{sol} = T_{sol}(\tau < \tau_c) - T_{sol}(\tau > \tau_c) \quad (2)$$

Where $T(\lambda, \tau)$ is the recorded percentage transmittance at a particular wavelength and temperature, ϕ_{lum} is the standard luminous efficiency function for the photopic vision of human eyes,³⁵ and ϕ_{sol} is the solar irradiance spectrum for air mass 1.5 (corresponding to the Sun standing 37° above the horizon).³⁶

Results and discussion

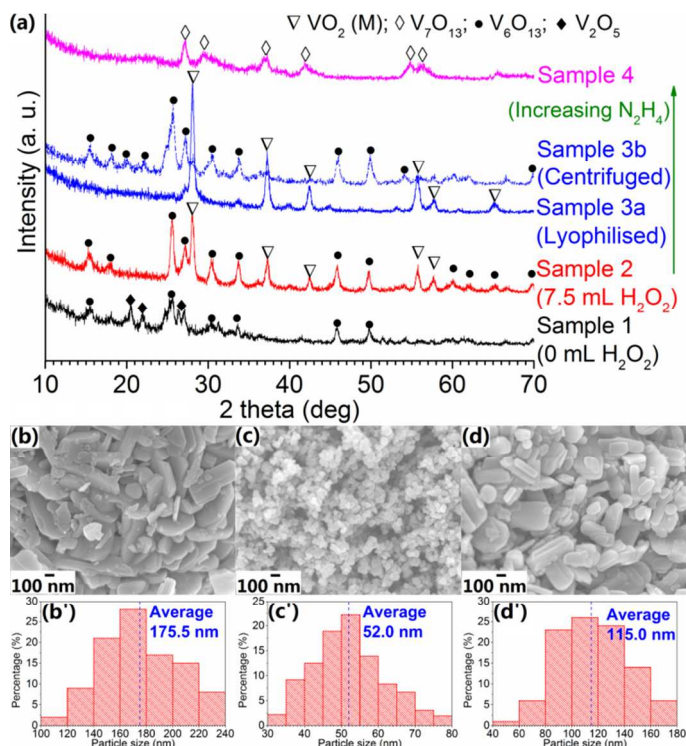


Fig. 1 (a) XRD patterns of samples 1-4; (b-d) FESEM images of samples 1, 3a and 3b respectively; (b'-d') histograms showing corresponding particle size distribution analyses.

Chemical reaction suggests that V_2O_5 is reduced by N_2H_4 according to the following scheme: $2V_2O_5 + N_2H_4 \rightarrow 4VO_2 + 2H_2O + N_2$. Sample 1 was made by dispersing 182.0 mg of V_2O_5 in 15.0 mL of deionized water and hydrazine was added in stoichiometry (25 μ L). **Fig. 1a** shows that only V_6O_{13} and V_2O_5 are present in the annealed sample, possibly because V_2O_5 has a poor solubility in water, hence the produced Sample 1 powder remained to have a large particle size of 175.5 nm (**Fig. 1b**). With the addition of hydrazine as reducing agent, only partial reduction took place and formed a mixture of V_6O_{13} and V_2O_5 during annealing, as the suggested reduction process for vanadium oxide is as following: $V_2O_5 \rightarrow V_3O_7 \rightarrow V_4O_9 \rightarrow V_6O_{13} \rightarrow VO_2 \rightarrow V_7O_{13} \rightarrow V_6O_{11} \rightarrow V_5O_9 \rightarrow V_4O_7 \rightarrow V_3O_5 \rightarrow V_2O_3$.³⁷ For further reduction to VO_2 , H_2O_2 was added to dissolve the starting material (V_2O_5 powder).

Sample 2 was made by adding 7.5 mL of H_2O_2 and after 2 h of reaction, the V_2O_5 - H_2O_2 precursor formed a reddish-brown sol which contained $V_2O_5 \cdot nH_2O$ NPs. The value of n was confirmed to be 2.0 by thermogravimetric analysis (TGA) and the method was reported in our previous publication.³⁸ With further addition of N_2H_4 with stoichiometric amount (90 μ L), the annealed Sample 2 was a mixture of VO_2 (M) and V_6O_{13} . The incomplete reduction could arise from the presence of residual H_2O_2 in the precursor which did not fully dissociate after 2 h of reaction, tending to re-oxidise the VO_2 (M) NPs to V_6O_{13} . Sample 3a was fabricated with increased addition of N_2H_4 (110 μ L), which produced a pure VO_2 (M) phase after heat treatment with high crystallinity and all the XRD peaks could be ascribed to JCPDS# 82-661. The FESEM images (**Fig. 1c**) show a much smaller particles size compared with Sample 1 (**Fig. 1b**) with an average of 52 nm, which proved the efficacy of H_2O_2 employed to dissolve the V_2O_5 raw powders. When N_2H_4 amount was further increased to 120 μ L (Sample 4), the presence of V_7O_{13} phase indicated over-reduction contributed by the excessive amount of N_2H_4 .

Meanwhile, Sample 3b was fabricated under the same condition as Sample 3a except that Sample 3b was dried via centrifugation but not freeze-dried. It can be observed that Sample 3b contains V_6O_{13} as major phase, with minor trace of VO_2 (M) in contrast with the highly crystalline Sample 3a with minor trace of undetermined impurity (**Fig. 1a**). This could be due to the residual H_2O_2 solvent content in the raw powder of Sample 3b which could not be fully removed even after centrifugation and drying in vacuum for 24 hours, and any remaining H_2O_2 would lead to incomplete reaction during the reduction of V_2O_5 to VO_2 . On the other hand, FESEM image of Sample 3b shows a mixture of plate-like and round shape morphologies of particles with an average size of 115 nm, and a large size distribution (**Fig. 1d**) compared with Sample 3a (**Fig. 1c**). It does suggest that freeze drying could keep the particles intact with much more uniform structures produced.¹⁷ As the solvent will be directly sublimed from solid to gas phase during freeze drying, the large capillarity force due to the solid-liquid transformation during ambient drying in Sample 3b will be eliminated, therefore the agglomeration issue which is common in the nanoparticles fabrication could be solved to large extent. Moreover, the reduced agglomeration ensures uniform heating during crystallisation, thereby reducing the amount of impurities and promoting the VO_2 phase formation as shown in **Fig. 1a**.

Fig. 2a shows the XRD patterns of the VO_2 (M) NPs synthesised using different amount of H_2O_2 and the sample designation is listed in **Table 2**. The general trend suggests that with increasing amount of H_2O_2 , the highest peaks' intensity reduces which related to lower crystallinity. As more H_2O_2 being added during precursor synthesis, a dramatic broadening of the characteristic peaks along (011)

orientation and declination of the peak intensity are observed starting from Sample 7 with 17.5 mL H_2O_2 . From the calculation using full-

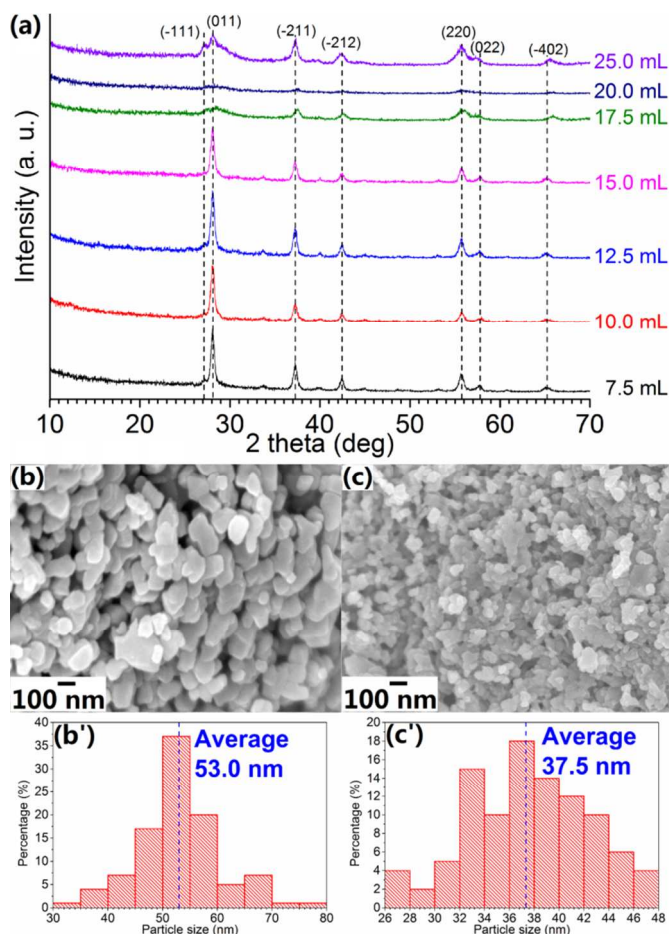


Fig. 2 (a) XRD patterns of VO_2 (M) NPs synthesised using different amount of H_2O_2 ; (b-c) FESEM images of Sample 4 and Sample 9, respectively; (b'-c') histograms showing corresponding particle size distribution analyses.

widths at half maxima (FWHM) at $2\theta \approx 28.0^\circ$, the crystallite size of Samples 3a, 4, 5 and 6 are estimated to be ~ 2 nm and this value is larger than that for Samples 7 to 9 (~ 1 nm). By lowering the V^{5+} concentration, smaller crystallites could be produced as well as small average particle size (**Table 2**).

Table 2 Summary of experimental data for synthesised VO_2 NPs

Sample no.	Amount of H_2O_2 (mL)	τ_c ($^\circ$ C)	$\Delta\tau_c$ ($^\circ$ C)	L_H (J/g)	L_C (J/g)	Average particle size [‡]
3a	7.5	64.1	4.3	25.66	31.88	52 nm
3c[#]	7.5	64.5	4.5	31.85	36.76	53 nm
4	10.0	64.2	5.6	19.54	27.23	53 nm
5	12.5	64.1	5.3	21.44	27.16	53 nm
6	15.0	65.8	5.5	11.95	21.24	55 nm
7	17.5	46.9	30.4	4.49	2.33	38 nm
8	20.0	43.8	35.1	3.17	0.57	37 nm
9	25.0	49.7	32.4	3.94	3.12	37 nm
Reference [§]	N. A.	68.0	2.5	38.70	41.87	50 μ m

L_H and L_C represent specific latent heat during heating and cooling stages.

[#] Sample 3c was made under the same condition as Sample 3a, except that it was heat treated at 650° C.

ARTICLE

§ The reference sample was tested using the commercial VO₂ (M) powder as purchased from Alfa Aesar, with particle size of ~ 50 μm.

‡ The average particle sizes were obtained from respective FESEM images.

According to the aggregative growth model constructed by Bogush and Zukoski, the size of final particles is directly proportional to the precursor concentration and inversely proportional to the nucleus size.³⁹ These explain the larger average particle size in Samples 3-6 and this agrees well with the mechanism of the Stöber process.⁴⁰ The above-mentioned finding is supported by the sudden change in the average particle sizes, which are listed in **Table 2**. Li et. al.²⁴ suggested that grain size has great influence on thermal behaviours of VO₂ NPs, and smaller particle size leads to lower phase transition temperature (τ_c), both of which could be observed in this study (**Table 2**). **Table 2** also records that smaller average particle size leads to an enlarged hysteresis width ($\Delta\tau_c$) and a much lower latent heat (L_H/L_C) for phase transition.⁴¹⁻⁴³

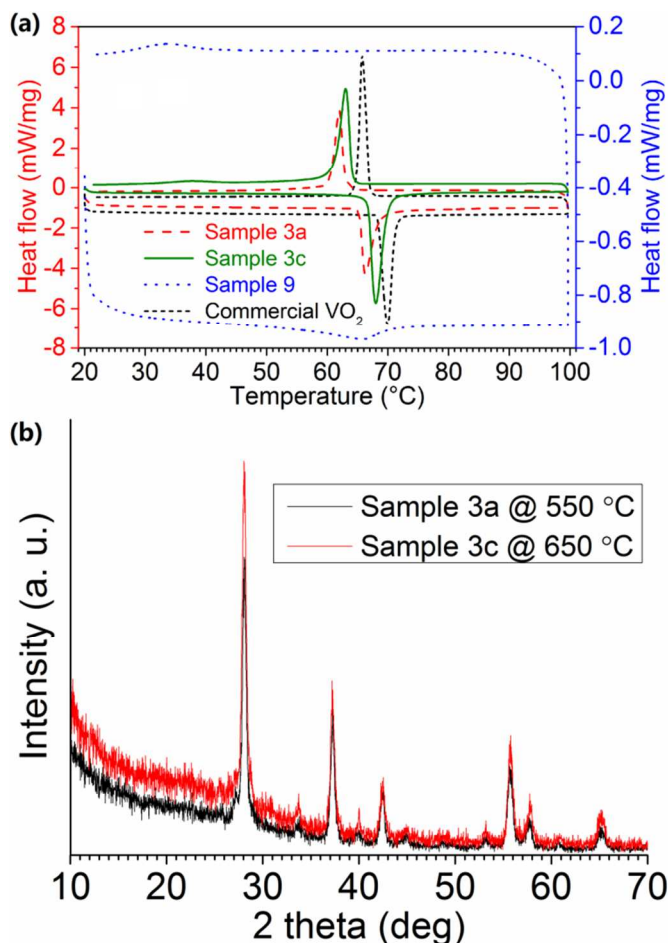
The phase transition of VO₂ (M) NPs was examined by DSC. By plotting the heat flow rate against temperature, a peak was observed in both the heating and cooling stages, forming a hysteresis loop, thereby indicating the first-order MIT in the VO₂ (M) NPs. The DSC graphs for Samples 3a, 3c, 9 and commercial VO₂ (M) powder (~ 50 μm) are shown in **Fig. 3a**. τ_c is calculated as the mean value of the heating and cooling peaks, and the difference between the two will be $\Delta\tau_c$. L_H/L_C is calculated as the area under each peak individually. The synthesised VO₂ (M) NPs are found to exhibit MIT at 64-66 °C, which is slightly lower than that for commercial VO₂ (M) at 68 °C (**Table 2**). This should be mainly due to the reduced particle size as a result of

Fig. 3 (a) DSC graphs of Samples 3a, 3c, 9 and commercial VO₂, the respective latent heat of phase transitions can be found in Table 2 ; (b) XRD patterns of Samples 3a (black line) and 3c (red line).

the solution-based synthesis route via freeze drying. The experimental data also follows the general phase transition mechanism as described in the literatures.^{44, 45}

Fig. 3a reveals that Sample 3a has much sharper and more distinct peaks than Sample 9, indicating a much greater crystallinity in the sample. This result is consistent with XRD observations (**Fig. 2a**). The small $\Delta\tau_c$ in Sample 3a signifies a quick response to the external stimuli, whereas the broadened peaks with large $\Delta\tau_c$ in Sample 9 represents a supercooling effect.⁴⁶ This might be due to that with lower vanadium concentration in the precursor, the annealed sample tends to have much smaller grain size and reveals much lower crystallinity as shown by the calculated latent heat for phase transition (**Table 2**), therefore having a slower response to the changes in the environment. Much smaller grain size and lower crystallinity in the sample may lead to a much lowered phase transition temperature, which is similar to the trend shown in the literature.²⁴

The precursor powder dried from 7.5 mL H₂O₂ synthesis was also annealed at 650 °C to obtain VO₂ (M) NPs with higher crystallinity (Sample 3c). This is evident from DSC and XRD (**Fig. 3a-b**), whereby Sample 3c had a higher latent heat during phase transition and a greater relative intensity of the diffraction peaks respectively.



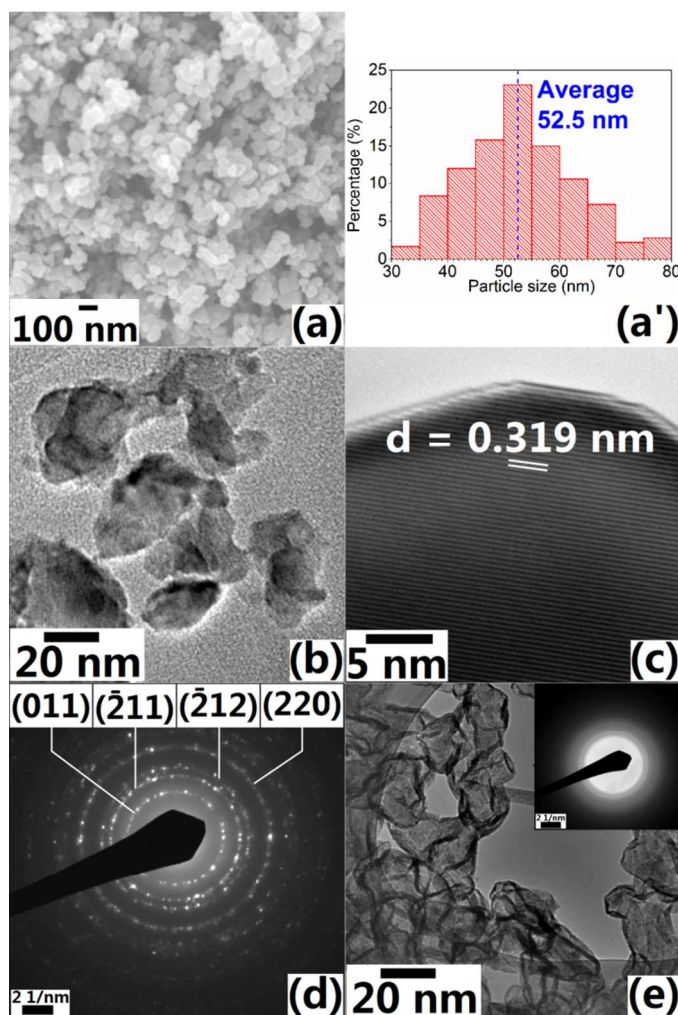


Fig. 4 (a) FESEM, (b) TEM, (c) HRTEM images and (d) the SAED pattern of Sample 3c; (a') histogram showing particle size distribution analysis; (e) TEM image of Sample 9 and its SAED pattern (inset).

FESEM image (Fig. 4a) shows that the particle size of Sample 3c does not differ much from that of Sample 3a (Fig. 1c). TEM image (Fig. 4b) of Sample 3c shows that VO₂ (M) NPs size is approximately 50 nm with little agglomeration and it is consistent with particle size distribution histogram (Fig. 4a') measured from Fig. 4a. HRTEM image (Fig. 4c) of Sample 3c indicates that the inter-plane distance for the nanocrystals is 0.319 nm, which matches well with the data for (011) orientation in JCPDS# 82-661 ($d_{011} = 0.320$ nm as indicated in standard database), this further confirms that the formed phase of the NPs is VO₂ (M); the corresponding SAED pattern (Fig. 4d) shows that the as-synthesised NPs are polycrystalline. On the other hand, TEM image of Sample 9 (Fig. 4e) shows that the particle size is smaller than that of Sample 3c, but the diffraction rings in its SAED pattern are not distinguishable, this indicates poor crystallinity of the sample 9 and this observation is consistent with XRD patterns (Fig. 2a). Thermal analysis for Sample 3c shows that the latent heat for phase transition of the sample is close to that of the commercial VO₂ (M) powder as purchased from Alfa Aesar, indicating similar crystallinity in the synthesised sample.

Fig. 5 displays the transmittance spectra of the casted film at 20 °C and 90 °C, as well as the hysteresis loop obtained at the fixed wavelength of 2500 nm. Since Sample 3c powder has the best

crystallinity and it was casted into a foil (with a powder loading of VO₂:PVP = 1:2 by mass), it has a deep bronze colour and renders thermochromic performance of $T_{lum} = 35^\circ\text{C}$ and $\Delta T_{sol} = 6.8\%$ (Fig. 5). The NIR transmittance contrast at $\lambda = 2500$ nm is $\sim 40\%$, this means the sample has high NIR modulating ability, which is an important factor of thermochromism. The hysteresis loop shows $\Delta\tau_c = 5^\circ\text{C}$, which is comparable to that of Sample 3c powder (Table 2); while further confirming the high crystallinity of Sample 3c, the fast response to the testing temperatures also signifies the practical application of VO₂ (M) NPs in the field of smart window coatings. However, the casted film has a slightly higher τ_c of 67.5 °C as compared to Sample 3c powder (64.5 °C), this might be because after casting, the grains get closer to each other due to the binding effect of PVP, thus showing the similar effect as agglomeration, and hence giving rise to a slightly higher τ_c .

Conclusions

In this study, VO₂ (M) NPs were synthesised by hydrazine reduction followed by freeze drying and annealing. Careful control of hydrazine

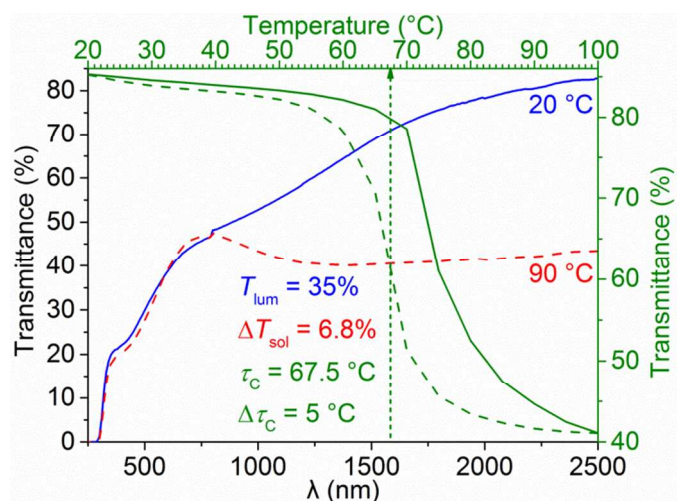


Fig. 5 Transmittance spectra of the casted film made from Sample 3c at 20 °C (blue curve) and 90 °C (red curve), as well as the hysteresis loop obtained at $\lambda = 2500$ nm (green curves).

amount is required to produce pure VO₂ (M) phase in the final samples. Freeze drying effectively keeps NPs well-separated in precursor powder, which leads to the formation of the VO₂ (M) NPs of ~ 50 nm. With more solvent in precursors, the average particle size is reduced from ~ 53 nm to ~ 37.5 nm; τ_c shows a general decreasing trend from 65.8 °C to 43.8 °C, while $\Delta\tau_c$ is enlarged from 4.3 °C to 35.1 °C. With a higher vanadium concentration, crystallinity and latent heat for phase transition of the samples can be improved. The freeze-dried sample (with 7.5 mL H₂O₂ in precursor) annealed at 650 °C has high crystallinity with a particle size of ~ 53 nm and $\tau_c = 64.5^\circ\text{C}$. Its latent heat for phase transition is ~ 36.76 J/g, which is close to the commercial VO₂ (M) powder (~ 41.87 J/g) as purchased from Alfa Aesar.

Acknowledgements

This research is supported by the Singapore National Research Foundation under CREATE programme: Nanomaterials for Energy and Water Management and Singapore Ministry of Education (MOE) Academic Research Fund Tier 1 RG101/13.

The XRD, FESEM and TEM characterizations were performed at the Facility for Analysis, Characterization, Testing and Simulation (FACTS) in Nanyang Technological University, Singapore.

Notes and references

^a School of Materials Science and Engineering, Nanyang Technological University, 50 Nanyang Avenue, (Singapore) 639798

^b Energy Research Institute @ NTU, Nanyang Technological University, 50 Nanyang Drive, (Singapore) 637553

^c Singapore Centre on Environmental Life Sciences Engineering (SCElse), Nanyang Technological University, 60 Nanyang Drive, (Singapore) 637551

^d Casali Institute of Applied Chemistry, Edmund Safra Campus, The Hebrew University, Jerusalem, (Israel) 91904

^e TUM CREATE Research Centre @ NTU, Nanyang Technological University, 62 Nanyang Drive, (Singapore) 637459

* Corresponding author: Dr Long Yi, E-mail: longyi@ntu.edu.sg

- M. K. Liu, H. Y. Hwang, H. Tao, A. C. Strikwerda, K. B. Fan, G. R. Keiser, A. J. Sternbach, K. G. West, S. Kittiwatanakul, J. W. Lu, S. A. Wolf, F. G. Omenetto, X. Zhang, K. A. Nelson and R. D. Averitt, *Nature*, 2012, **487**, 345.
- M. M. Qazilbash, M. Brehm, B.-G. Chae, P.-C. Ho, G. O. Andreev, B.-J. Kim, S. J. Yun, A. V. Balatsky, M. B. Maple, F. Keilmann, H.-T. Kim and D. N. Basov, *Science*, 2007, **318**, 1750.
- C. Kübler, H. Ehrke, R. Huber, R. Lopez, A. Halabica, R. F. Haglund and A. Leitenstorfer, *Phys. Rev. Lett.*, 2007, **99**, 116401.
- P. Kiri, G. Hyett and R. Binions, *Adv. Mat. Lett.*, 2010, **1**, 86.
- X. Cao, N. Wang, S. Magdassi, D. Mandler and Y. Long, *Sci. Adv. Mater.*, 2014, **6**, 558.
- C. Liu, N. Wang and Y. Long, *Appl. Surf. Sci.*, 2013, **283**, 222.
- S. Chen, L. Dai, J. J. Liu, Y. F. Gao, X. L. Liu, Z. Chen, J. D. Zhou, C. X. Cao, P. G. Han, H. J. Luo and M. Kanehira, *Phys. Chem. Chem. Phys.*, 2013, **15**, 17537.
- E. Strelcov, Y. Lilach and A. Kolmakov, *Nano Lett.*, 2009, **9**, 2322.
- A. Boscolo, E. Menosso, B. Piuze and M. Toppano, in *Device Applications of Nonlinear Dynamics*, eds. S. Baglio and A. Bulsara, Springer Berlin Heidelberg, 2006, 139.
- M. Nakano, K. Shibuya, D. Okuyama, T. Hatano, S. Ono, M. Kawasaki, Y. Iwasa and Y. Tokura, *Nature*, 2012, **487**, 459.
- G. V. Jorgenson and J. C. Lee, *Sol. Energy Mater.*, 1986, **14**, 205.
- E. E. Chain, *Appl. Opt.*, 1991, **30**, 2782.
- F. A. Chudnovskii, A. L. Pergament, D. A. Schaefer and G. B. Stefanovich, *Proceedings of SPIE*, 1996, 80.
- C. Liu, X. Cao, A. Kamyshny, J. Y. Law, S. Magdassi and Y. Long, *J. Colloid Interface Sci.*, 2014, **427**, 49.
- Z. Chen, Y. F. Gao, L. T. Kang, C. X. Cao, S. Chen and H. J. Luo, *J. Mater. Chem. A*, 2014, **2**, 2718.
- X. K. Qian, N. Wang, Y. F. Li, J. H. Zhang, Z. C. Xu and Y. Long, *Langmuir*, 2014, **30**, 10766.
- X. Cao, N. Wang, J. Y. Law, S. C. J. Loo, S. Magdassi and Y. Long, *Langmuir*, 2014, **30**, 1710.
- Y. Zhou, Y. F. Cai, X. Hu and Y. Long, *J. Mater. Chem. A*, 2014, **2**, 13550.
- Y. Zhou, Y. F. Cai, X. Hu and Y. Long, *J. Mater. Chem. A*, 2014 (Accepted, DOI: 10.1039/C4TA05035E).
- Y. F. Gao, S. B. Wang, H. J. Luo, L. Dai, C. X. Cao, Y. L. Liu, Z. Chen and M. Kanehira, *Energy Environ. Sci.*, 2012, **5**, 6104.
- C. M. Zheng, X. M. Zhang, J. H. Zhang and K. R. Liao, *J. Solid State Chem.*, 2001, **156**, 274.
- Y. F. Gao, S. B. Wang, L. T. Kang, Z. Chen, J. Du, X. L. Liu, H. J. Luo and M. Kanehira, *Energy Environ. Sci.*, 2012, **5**, 8234.
- L. Dai, S. Chen, J. J. Liu, Y. F. Gao, J. D. Zhou, Z. Chen, C. X. Cao, H. J. Luo and M. Kanehira, *Phys. Chem. Chem. Phys.*, 2013, **15**, 11723.
- M. Li, X. Wu, L. Li, Y. X. Wang, D. B. Li, J. Pan, S. J. Li, L. T. Sun and G. H. Li, *J. Mater. Chem. A*, 2014, **2**, 4520.
- S. D. Ji, F. Zhang and P. Jin, *Sol. Energy Mater. Sol. Cells*, 2011, **95**, 3520.
- J. Zou, Y. G. Peng and H. Lin, *J. Mater. Chem. A*, 2013, **1**, 4250.
- L. F. Su, L. Miao, S. Tanemura and G. Xu, *Sci. Technol. Adv. Mater.*, 2012, **13**, 035003.
- O. A. Shlyakhtin and Y.-J. Oh, *J. Electroceram.*, 2009, **23**, 452.
- S. R. Mukai, H. Nishihara and H. Tamon, *Catal. Surv. Asia*, 2006, **10**, 161.
- E. Baudrin, G. Sudant, D. Larcher, B. Dunn and J.-M. Tarascon, *Chem. Mater.*, 2006, **18**, 4369.
- G. Sudant, E. Baudrin, B. Dunn and J.-M. Tarascon, *J. Electrochem. Soc.*, 2004, **151**, A666.
- J. J. Xu and J. Yang, *Electrochem. Commun.*, 2003, **5**, 230.
- J. H. Harreld, W. Dong and B. Dunn, *Mater. Res. Bull.*, 1998, **33**, 561.
- W. Abdelwahed, G. Degobert, S. Stainmesse and H. Fessi, *Adv. Drug Deliv. Rev.*, 2006, **58**, 1688.
- G. Wysocki and W. S. Stiles, *Color Science: Concepts and Methods, Quantitative Data and Formulae*, Wiley, New York, Second Edition, 2000.
- Standard Tables of Reference, *Solar Spectral Irradiance: Direct Normal and Hemispherical on a 37° Tilted Surface*, Annual Book of ASTM Standards, 2012, G173-03.
- H. P. Ma and S. Q. Xu, *Rare Metal Mat. Eng.*, 2004, **33**, 317.
- N. Wang, S. Magdassi, D. Mandler and Y. Long, *Thin Solid Films*, 2013, **534**, 594.
- G. H. Bogush and C. F. Zukoski IV, *J. Colloid Interface Sci.*, 1991, **142**, 19.
- W. Stöber, A. Fink and E. Bohn, *J. Colloid Interface Sci.*, 1968, **26**, 62.
- R. Lopez, L. C. Feldman and R. F. Haglund, *Phys. Rev. Lett.*, 2004, **93**, 177403.
- E. U. Donev, R. Lopez, L. C. Feldman and R. F. Haglund, *Nano Lett.*, 2009, **9**, 702.
- K. Appavoo, D. Y. Lei, Y. Sonnefraud, B. Wang, S. T. Pantelides, S. A. Maier and R. F. Haglund, *Nano Lett.*, 2012, **12**, 780.
- R. Lopez, T. E. Haynes, L. A. Boatner, L. C. Feldman and R. F. Haglund, *Phys. Rev. B*, 2002, **65**, 224113.
- E. U. Donev, J. I. Ziegler, R. F. Haglund and L. C. Feldman, *J. Opt. A: Pure Appl. Opt.*, 2009, **11**, 125002.
- N. Wang, Y. Z. Huang, S. Magdassi, D. Mandler, H. Liu and Y. Long, *RSC Advances*, 2013, **3**, 7124.